Received: 24 May 2023 | Revised: 4 October 2023 | Accepted: 17 October 2023

DOI: 10.1002/eqe.4032

RESEARCH ARTICLE

WILEY

Seismic performance of the temple of Aphaia in Aegina island, Greece

Maria-Eleni Dasiou | **Christos G. Lachanas** | **Vasileios E. Melissianos** | **Dimitrios Vamvatsikos**

School of Civil Engineering, National Technical University of Athens, Athens, Greece

Correspondence
Maria-Eleni Dasiou, School of Civil Engineering, National Technical University of Athens, Heroon Polytehneiou 9, Politehneioupoli, 15772 Zografos, Athens, Greece.
Email: medasiou@mail.ntua.gr

Funding information
Greek national funds through the Operational Program Competitiveness, Entrepreneurship and Innovation, Project ARCHYTAS, Grant/Award Number: T1EDK-00956; European Commission through the Horizon 2020, Project "YADES", Grant/Award Number: 872931

Abstract

The seismic performance assessment of the ancient Temple of Aphaia in Aegina island, Greece, is presented. The Temple of Aphaia was erected around 500BC using porous limestone and is one of the most characteristic examples of Doric architecture. The assessment is performed within a performance-based framework using state-of-the-art tools of earthquake engineering. In the first part, the seismic hazard of the site was calculated using the European Seismic Hazard Model and hazard-consistent records were selected. Then, the Temple was scanned by drone and the point cloud was used to develop the numerical structural model. The Temple was analyzed using the discrete element method. Appropriate engineering demand parameters and limit state thresholds were defined. Fragility curves for the structural elements, namely, columns and architraves, of the Temple were computed via multi-stripe analysis. Finally, the seismic risk of the Temple was evaluated using long-term estimates in terms of return periods of exceeding limit states and total loss. The outcomes of the study offer valuable information to engineers, architects, and archaeologists regarding the current status of the monument in terms of identifying its most vulnerable elements and allowing the prioritization of short- and long-term restoration actions.

KEYWORDS

ancient temple, discrete element method, earthquake engineering, fragility analysis, performance assessment, risk estimation

1 | INTRODUCTION

The protection and conservation of cultural heritage (CH) assets is a duty for modern societies because monuments are part of history and reflect continuous human activity and creativity. There is, also, heightened public awareness on the topic, and thus international policy documents are in effect, such as the European Framework for Action on Cultural Heritage[1] and the Council of Europe's Technical Co-Operation and Consultancy Programme.[2] It is generally

acknowledged that monumental structures are continuously exposed to natural and man-made hazards. Among the natural hazards, earthquakes are the most prominent for Greece, in terms of threatening the structural integrity.

The seismic assessment of CH assets is a tricky exercise due to non-negligible difficulties and uncertainties on material properties, numerical modeling, and representation of the contact between structural elements. At this point, it should be noted that there is significant research effort on masonry buildings, churches, towers, etc.[3–7] On the other hand, when it comes to ancient monuments that are spinal structures without mortar connecting the elements, research can be limited. It is a difficult objective due to the highly non-linear dynamic behavior of these structures when subjected to earthquake excitation. In such a case, the structural elements respond by experiencing mainly rocking and secondary sliding, rather than more conventional modes of deformation. Several researchers have studied the rocking response of rigid bodies, for example,[8–15] while testing has confirmed that even trivial changes in the geometry, for example, due to local fracture of the element's edge, may significantly modify the response.[16]

The seismic analysis of ancient temples has almost exclusively focused on the assessment of single free-standing columns, given their significant vulnerability to earthquakes, for example.[16–24] Contrarily, studies of large temple sub-assemblages and/or an entire temple are scarce. For example, Dasiou and Psycharis[25] have examined the seismic response of a part of the Temple of Hephaestus in Athens, Greece, while Dasiou et al.[26] have numerically analyzed the response of the Cella Walls of the Parthenon in Athens, Greece. These studies, as well as those dealing with single columns and colonnades, either focus on the development of the numerical model or go one step forward to calculate the fragility curves.

Herein, a seismic assessment of the Temple of Aphaia on the island of Aegina in Greece is presented, featuring all stages of a Performance-Based Earthquake Engineering[27] study: (a) seismic hazard assessment and selection of hazard-consistent natural ground motion records, (b) photogrammetric survey, (c) numerical modeling of the structure, (d) definition of engineering demand parameters, limit states, and capacity thresholds, (e) seismic response of the Temple under single ground motions, (f) seismic fragility assessment, and (g) seismic risk assessment in the form of element-by-element long-term estimates of limit-state occurrence.

2 | HISTORY AND TYPOLOGY OF THE MONUMENT

A temple dedicated to the mother-goddess Aphaia was built around 560BC within a sanctuary complex on the island of Aegina, Greece, located southwest of Athens. It was made of limestone and was demolished around 500BC after it suffered significant damage caused by fire. At the same location, a new Temple of porous limestone (porolite) was erected and used until it was abandoned during the 2nd century BC. In modern times, archaeological excavations were carried out around 1810, when the sculptures were removed, which are now exhibited at the Glyptothek in Munich, Germany. Systematic excavations were also performed in 1901 and during 1964–1981 by the German Archaeological Institute of Athens. Historical reports on the excavations during the 19th and 20th centuries are provided by Webster,[28] Gill,[29] and Furtwängler et al.[30]

From the archive of the German Archaeological Institute of Athens it is evident that during the period of 1805–1875, the walls of the Cella, the inner colonnades and some columns of the outer colonnade were not preserved in place and that on a number of columns the strengthening technique of steel rings was applied. The most extensive interventions and restoration works were carried out under the supervision of A. Orlandos and E. Stikas during 1952–1960, when the temple was restored to the form found nowadays by removing the steel rings and restoring parts of the internal and external colonnades and the Cella. A small intervention on the monument took place in 2010, when the architrave on the portal wall of the Cella, which was initially reinstalled in 1957, was strengthened. Today, the Ephorate of Antiquities of Piraeus and Islands of the Ministry of Culture, Hellenic Republic, is responsible for the preservation of the monument.

The Temple of Aphaia (Figure 1) is considered one of the most important and well-preserved monuments of archaic architecture. The Temple is founded on a three-layered crepidoma (i.e., stone foundation) and consists of the Opisthodomos (posterior), the Cella (central), the Pronaos (anterior), and the external colonnade. It is a peripteral Doric order temple with 12 columns on the long side and 6 on the short side (corner columns are double-counted). The side views of the temple are shown in Figure 2. The dimensions of the stylobate (base) are 30.55 m × 15.50 m and the Cella is approximately 22.50 m long and 8.00 m wide. Initially the external colonnade of the temple consisted of six columns at the narrow sides and twelve on the wide. Nowadays, on the north and south side, nine and seven columns respectively can be found, while on the west side only three remain intact. On the east side of the temple all columns are still standing. The total height of the columns of the external colonnade is 5.30 m and the diameter at the base is 1.00 m. The columns

FIGURE 1 The Temple of Aphaia [courtesy of the authors and the Directorate of Restoration of Ancient Monuments, Ministry of Culture, Hellenic Republic].

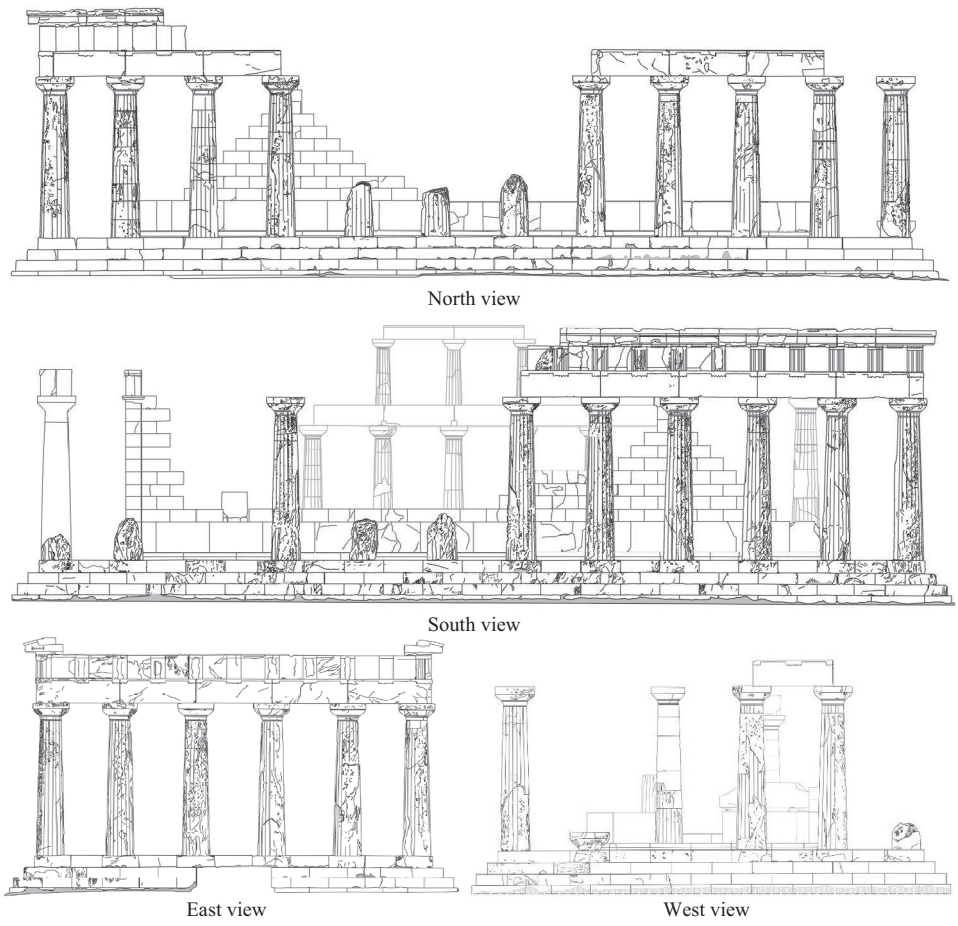

FIGURE 2 Side views of the Temple of Aphaia [courtesy of the authors and the Directorate of Restoration of Ancient Monuments, Ministry of Culture, Hellenic Republic].

are tapering towards the top with the diameter decreasing at the top to 0.70 m. The average dimensions of the architraves are 2.57 × 0.52 × 0.83 m (length x width x height).

The remains of the Temple nowadays include free-standing monolithic columns (Figure 3A), free-standing multi-drum column (Figure 3B), a colonnade of four columns with architraves (Figure 3C), colonnades of two columns with architrave (Figure 3D), a multi-drum column connected to a part of the Cella wall with an architrave (Figure 3E), corner colonnade with architraves (Figure 3F), and two-level colonnades with architraves in the Cella (Figure 3G). These sub-assemblages are structurally independent. All columns are monolithic unless otherwise stated and the architraves consist of two parts

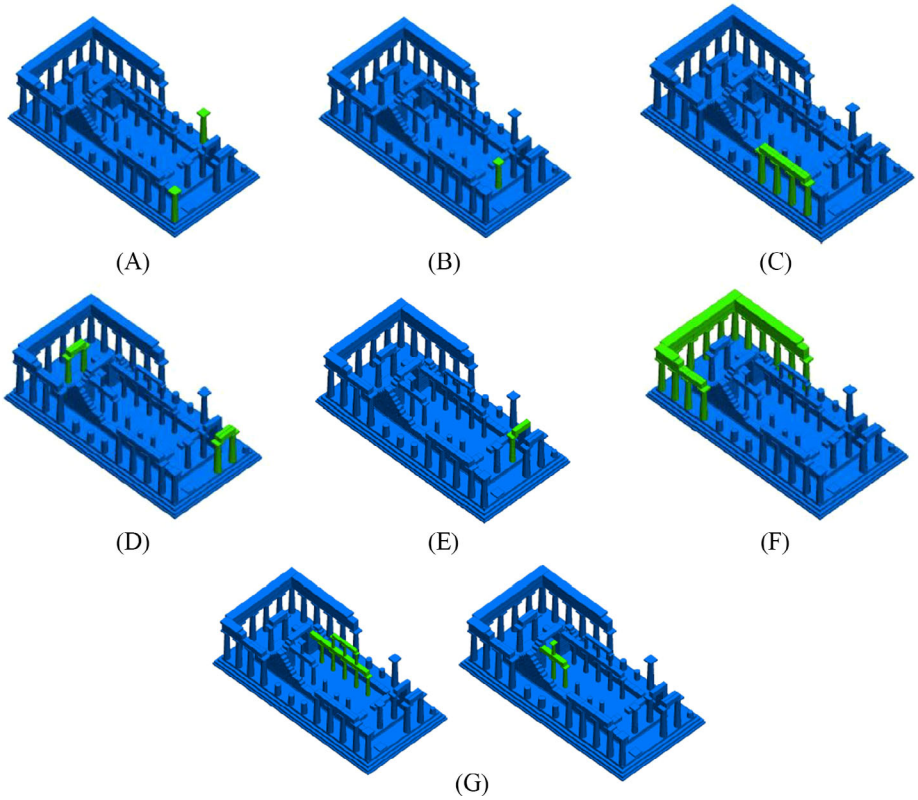

FIGURE 3 Sub-assemblages of the Temple of Aphaia: (A) free-standing monolithic columns, (B) free-standing multi-drum column, (C) a colonnade of four columns with architraves, (D) colonnades of two columns with architrave, (E) a multi-drum column connected to the Cella wall with an architrave, (F) corner colonnade with architraves, (G) two-level colonnades with architraves in the Cella.

(one internal and one external) without connections. There is evidence that connectors were used in the architraves but today they are not found. Remains of the frieze (upper part of the entablature) can be found in the corner colonnade (Figure 3F). As an interesting remark, the Temple of Aphaia is one of the very few where the two-level colonnade of the Cella has survived till today. Overall, the monument is in a moderate level of preservation and its remnants have suffered non-negligible damage due to natural and man-made actions and hazards. Cellular or cavernous erosion of the material by environmental factors, cracks due to mechanical stress, material damage, and calcification can be observed.

3 | SEISMIC HAZARD

The seismic hazard at the site of the Temple of Aphaia, with coordinates N 37 45.274 and E 23 32.018, was computed using the OpenQuake engine[31] of the Global Earthquake Model Foundation. The probabilistic seismic hazard analysis (PSHA)[32] calculations were carried out using the 2013 European Seismic Hazard Model (ESHM13) developed within the SHARE project.[33] To reduce the computational burden, only the area source model and the ground motion prediction equation of Boore and Atkinson[34] were used. As the temple is founded directly on rock, a shear wave velocity in the top 30 m of the ground of $V_{s,30} = 800$ m/s was considered in the calculations.

The intensity measure (IM) allows the seismic hazard information to flow from the seismological analysis to the structural analysis. $AvgS_a$ is selected as IM and is defined as the geometric mean of the spectral accelerations over a range of periods,[35,36] herein set from 0.1 to 1.5 s. Rocking rigid bodies, such as the structural elements of an ancient temple, do not possess natural modes in the classic sense because the period of vibration is amplitude-dependent.[8] Thus, the fundamental period of vibration cannot be defined. Nevertheless, the selected range of periods is a reasonable engineering assumption as lower period ordinates affect early damage, while longer periods are better correlated with overturning.[37] Moreover, $AvgS_a$ is proposed by Lachanas et al.[38] as an efficient and sufficient IM for the case of rocking structures, still having the disadvantage of selecting the proper period range per block case. By employing PSHA with $AvgS_a$ as IM, the

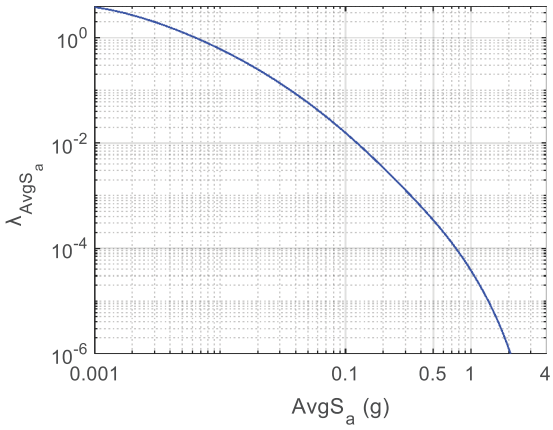

FIGURE 4 Mean hazard curve for the site of the Temple of Aphaia.

TABLE 1 Hazard levels considered for the multi-stripe analysis and for selection/scaling of ground motions.

Hazard level	λ_{AvgS_a}	P_{50}	Return period (years)	$AvgS_a$ (g)
1	0.0045	20%	225	0.18
2	0.0021	10%	475	0.25
2a	0.0009	4.13%	1145	0.35[a]
3	0.0004	2%	2475	0.48
4	0.0002	1%	4975	0.63

[a]Scaled records of Hazard Level 2.

computed mean hazard curve is shown in Figure 4, presenting the mean annual frequency (MAF), denoted as λ_{AvgS_a}, of exceeding any level of $AvgS_a$.

Four hazard levels are considered for the record selection process and for performing multi-stripe analysis (MSA).[39] They are listed in Table 1 where the probability of exceedance in 50 years (P_{50}), the corresponding return period, and the $AvgS_a$ value per level for the site of the Temple are presented. Hazard Level 2 corresponds to a P_{50} of 10%, which is the hazard level that is employed for the design of conventional structures.[40] The rest of the selected hazard levels correspond either to more frequent (Hazard Level 1) or less frequent (Hazard Levels 3, 4) ones in order to cover the full range of structural response via MSA. Then, the Conditional Spectrum-based ground motion record selection using $AvgS_a$, as developed by Kohrangi et al.,[41,42] was performed. In particular, the algorithm of Jayaram et al.[43] was employed and 11 ground motions from the PEER-NGA database[44] were selected per hazard level, each one corresponding to the $AvgS_a$ of the predefined hazard level after being multiplied with a proper scale factor. During later analysis, an improved coverage was found to be useful between Hazard Levels 2 and 3. Therefore, an additional stripe (Hazard Level 2a) was employed by taking the ground motions of Hazard Level 2 and applying a minor rescaling to reach the level of $AvgS_a = 0.35$ g. This frugal selection of five hazard levels and 11 records is dictated by the complexity of the structural model, with a single run needing almost 24 h of computer time. Still, this is considered adequate to offer a reliable representation of the monument response.

4 | STRUCTURAL MODEL

4.1 | Numerical modeling

Ancient Greek temples consist of independent building stones that are placed on top of each other without any connecting material (e.g., mortar). Due to this modular configuration, their seismic response differs significantly from that of modern structures and is characterized by rocking and/or sliding of the stones independently or in groups. Particularly in cases of columns and colonnades, rocking is the dominant form of response to strong seismic excitations, while sliding of the drums is usually limited to the upper part of the columns, where significant accelerations develop, capable of overcoming

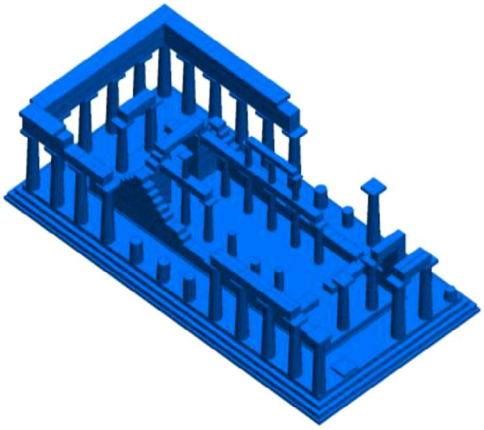

FIGURE 5 3D isometric view of the numerical model of the Temple of Aphaia.

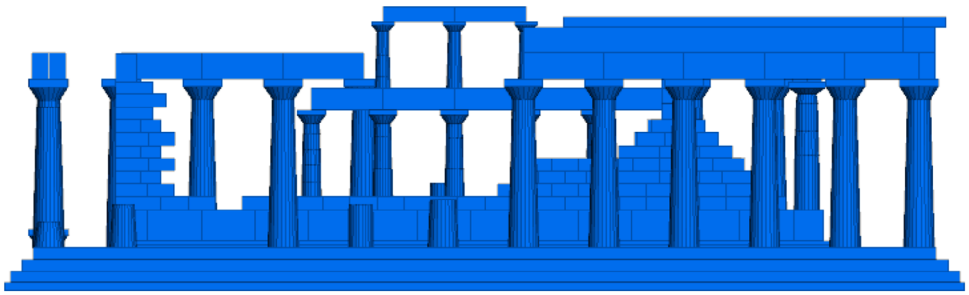

FIGURE 6 South view of the numerical model of the Temple of Aphaia.

frictional forces. Thus, the calculation of their response to seismic excitations cannot be carried out using conventional finite element software; previous research studies and comparisons with experimental results have shown that the Discrete Element Method (DEM) can predict the response of modular structures with sufficient accuracy.[22,26,45] In the current study, the code 3DEC by Itasca Consulting Group, Inc.[46] was employed. It is based on DEM and was originally developed for the analysis of rock masses, which are considered as a set of distinct solid bodies with boundary conditions simulating a discontinuity state; large displacements and rotations are allowed, including sliding between bodies, the opening of cracks, and complete detachment of bodies that were initially in contact. As the calculation process continues, the software detects new contacts, while in the areas where the rigid bodies are in contact, shear and axial force are calculated from the equilibrium equations of each body. Normal and shear stiffness were assigned at the joints using values obtained from literature test data on ancient multi-drum columns.[26,45] As a remark, it is noted that the examined ancient Temple is founded on rock and therefore soil-structure interaction does not affect the monument's response.

In order to obtain an accurate numerical model of the Temple in its present state, a photogrammetric survey was carried out. In specific, an Unmanned Aerial Vehicle (UAV) equipped with an ultra-high-definition camera (resolution 5472 × 3648 pixels) was deployed to take 2457 photos in total. The aerial photos were processed with reference to 24 GPS (Global Positioning System) photostable points and 57 photostable points set with a Total Station. Identification algorithms were applied to successive photographs in order to automatically detect homologous characteristic points on the surface of objects and render 3D coordinates on them. To this end, the 3D point cloud of the structure was constructed and was used for developing the numerical model. In specific, the point cloud obtained from the photogrammetric survey was used to create several sections of the Temple in horizontal and vertical planes in CAD software. The coordinates of each block were obtained and imported in 3DEC via appropriate input files. An overall 3D view of the developed numerical model is presented in Figure 5, while the four side views, namely, south, north, west, and east are shown in Figure 6–9, respectively. The model was developed using the geometry obtained from the photogrammetric survey in order to consider the current state of the monument. In more detail, missing parts of the stone blocks were cut of in the model, while the actual positions of the blocks were considered, that is, taking into account any measured dislocation of drums/columns and architraves, which are actual geometric defects. It is noted that minor cracks were not included in the model. In addition, the reliefs

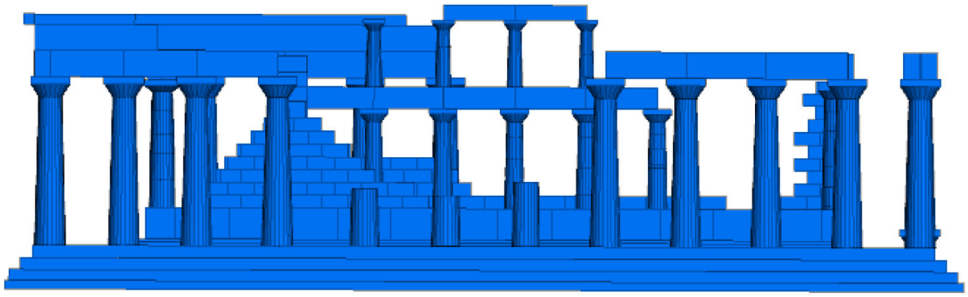

FIGURE 7 North view of the numerical model of the Temple of Aphaia.

FIGURE 8 West view of the numerical model of the Temple of Aphaia.

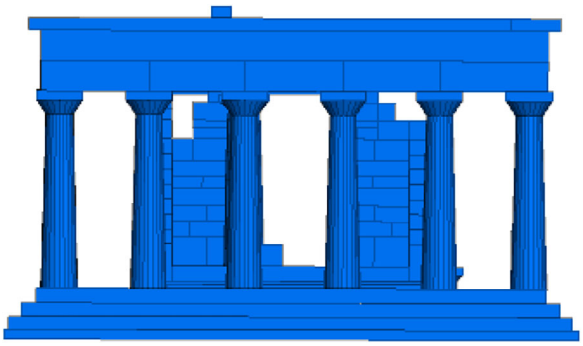

FIGURE 9 East view of the numerical model of the Temple of Aphaia.

of the architraves, the frieze, and the cornice, which are not structural elements and do not affect the dynamic behavior of the monument, were not simulated.

The Temple is made of porolite and since no experimental data was available, the material properties were obtained from the literature, where actually a large dispersion of values appears regarding the modulus of elasticity and Poisson's ratio. In our work, we statistically evaluated these values and adopted the average values for the modulus of elasticity (E = 70 GPa), the Poisson's ratio ($\nu = 0.25$) and density ($\rho = 2750$ kg/m^3). As mentioned previously, the 3DEC code locates the contacts between the rigid bodies and calculates the forces developed between them based on the elastic constants at the interfaces (coefficient of friction, stiffness modulus, etc.). For the simulation of the joints, the stiffness k of the contact elements was determined based on previous research[26,45]: $k_n = 5 \times 10^9$Pa/m in the direction perpendicular to the joint and $k_s = 1 \times 10^9$Pa/m parallel to the joint. In addition, a 10% mass-proportional damping at $\omega = 0.3$ Hz was considered. This damping value has been verified Dasiou et al.[26] using experimental measurements.

Despite the identification of distinct and structurally independent sub-assemblages that may comprise multiple elements, the seismic performance of the Temple was evaluated at the level of each structural element, namely, each column and architrave, each of which was assigned a unique identifier, as presented in Figure 10 and listed in Table 2. The deliberate decision to treat in structural terms each column and architrave separately offers higher fidelity, allowing us to define appropriate engineering demand parameters (EDPs), as well as respective demands and capacities, at the local element

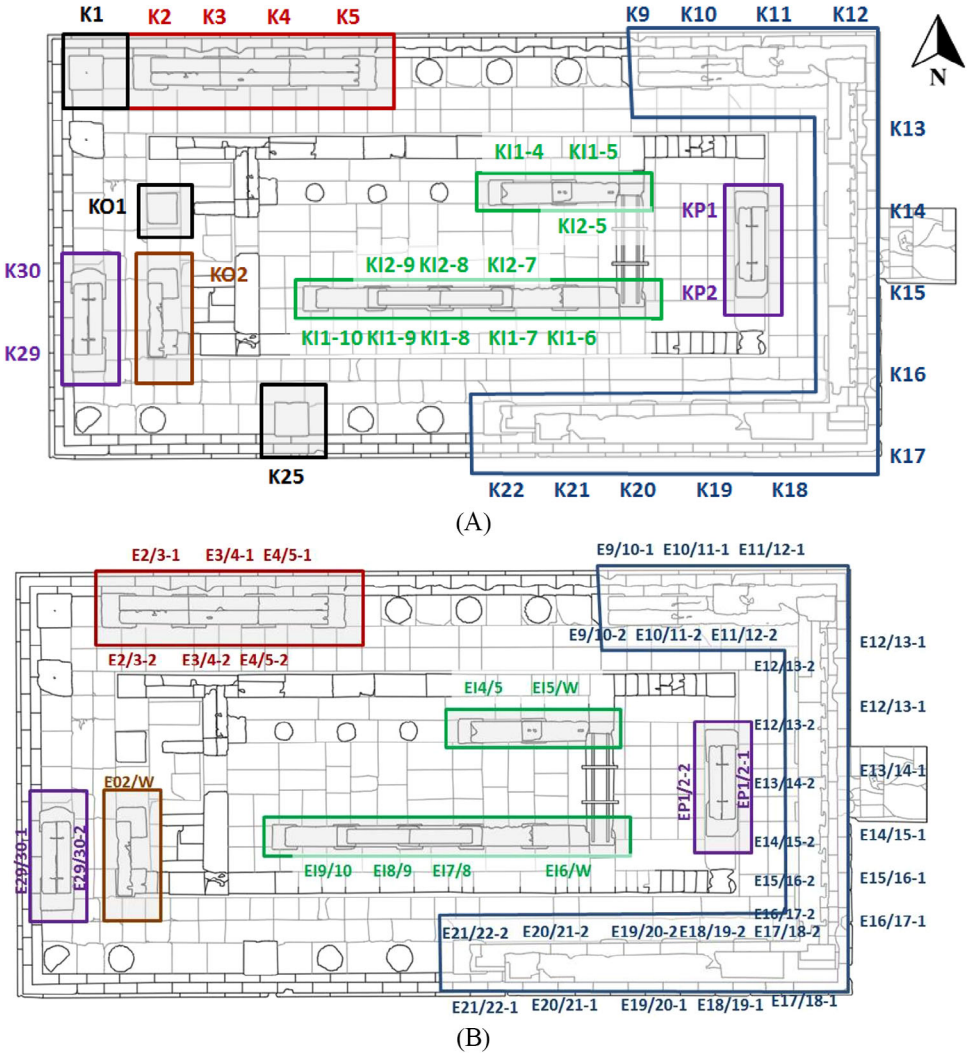

FIGURE 10 Nomenclature of (A) columns and (B) architraves in plan view (see also Table 2) [plot plan is courtesy of the authors and the Directorate of Restoration of Ancient Monuments, Ministry of Culture, Hellenic Republic].

TABLE 2 Nomenclature of structural elements.

Element	Notation	Element	Notation
Column of external colonnade	K	Architrave of external colonnade	E
Columns of Pronaos	KP	Architrave of Pronaos	EP
Column of Opisthodomos	KO	Architrave of Opisthodomos	EO
Column of internal colonnade – first level	KI1	Architrave of internal colonnade – first level	EI1
Column of internal colonnade - second level	KI2	Architrave of internal colonnade – second level	EI2

level, rather than at an entire sub-assemblage. As a final remark, it was revealed from the analyses that the rigid stone blocks comprising the Cella walls were only subject to minor displacements. Thus, they were exempted from further examination.

4.2 | Engineering demand parameters

EDPs are structural response values that can be used to evaluate the performance and estimate the damage of the structural and nonstructural components. In the case of ancient temples, where no connecting material is present, their seismic response is characterized by rocking and/or sliding of the columns and sliding of the entablature (i.e., mainly the

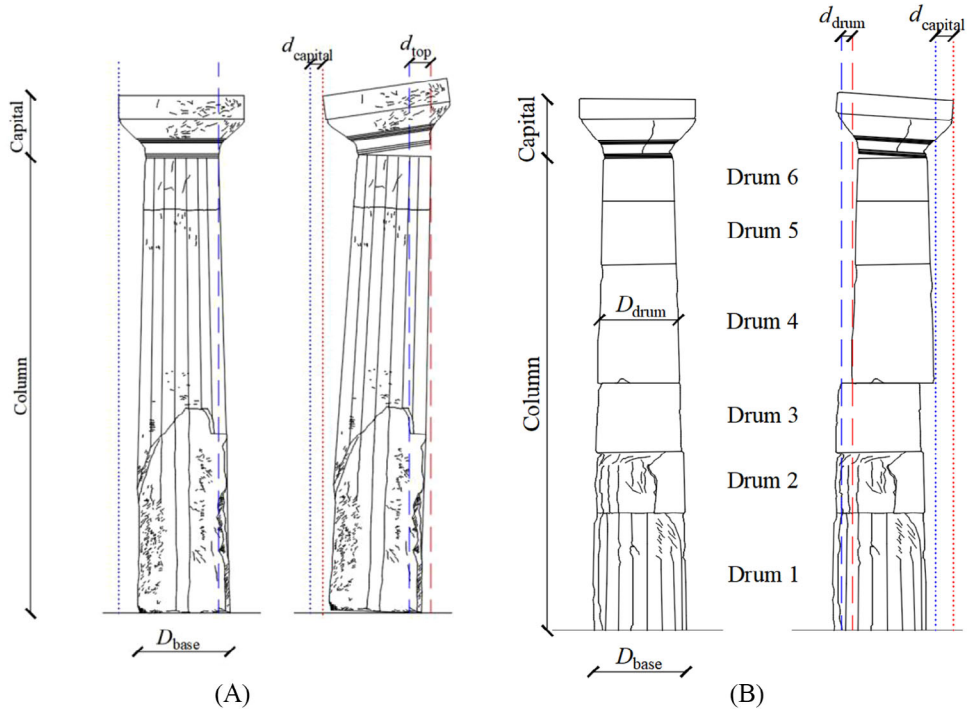

FIGURE 11 Definition of EDPs for (A) monolithic columns and (B) multi-drum columns. Blue vertical lines indicate the initial position of the blocks while red lines their displaced (peak or residual) position [drawings are courtesy of the authors and the Directorate of Restoration of Ancient Monuments, Ministry of Culture, Hellenic Republic].

architraves). In more detail, two EDPs in terms of displacement were introduced for the columns, namely, (a) the maximum value obtained during the dynamic excitation (δ_{max}) and (b) the residual value (δ_{res}) at the end of the excitation. It is noted that for both monolithic and multi-drum columns, the capital was treated as part of the column and not as an independent structural element. Thus, the normalized displacement δ (both in terms of δ_{max} and δ_{res}) for monolithic columns was calculated as:

$$\delta = \max\left(d_{\text{capital}}; d_{\text{top}}\right)/D_{\text{base}} \text{ for monolithic column} \tag{1}$$

where d_{capital} is the displacement of the capital, d_{top} is the displacement of the top of column, both with respect to their initial position, and D_{base} is the base diameter of the column (Figure 11A).

The normalized displacement δ (both δ_{max} and δ_{res}) for the multi-drum columns (Figure 11B) was calculated as:

$$\delta = \max\left(\frac{d_{\text{capital}}}{D_{\text{drum,u}}}; \left\{\begin{matrix}\frac{d_{\text{drum},N}}{D_{\text{drum},N,\text{u}}} \\ \vdots \\ \frac{d_{\text{drum},2}}{D_{\text{drum},2,\text{u}}} \\ \frac{d_{\text{drum},1}}{D_{\text{drum},1,\text{u}}}\end{matrix}\right\}; \frac{d_{\text{capital}}}{D_{\text{base}}}\right) \text{ for multi-drum column} \tag{2}$$

where $d_{\text{drum},i}$ is the displacement of the i-th drum and $D_{\text{drum},i,\text{u}}$ is the diameter of its respective underlying drum, $i = 1, 2, \ldots N$, with N being the total number of drums of the column.

Following the concept discussed for the columns, two EDPs were introduced for the entablature, namely, the transverse maximum (δ_{max}) and residual (δ_{res}) values of the dislocation of the block normalized by the architraves' bearing length (half width of the capital's abaqus). The normalized transverse displacement (both δ_{max} and δ_{res}) was computed as:

$$\delta = d_{\text{arc}}/A_b \text{ for architraves} \tag{3}$$

where d_{arc} is the transverse displacement of the architrave with respect to its initial position and A_b is the architrave bearing length that is equal to the half width of the capital abaqus W_a (Figure 12).

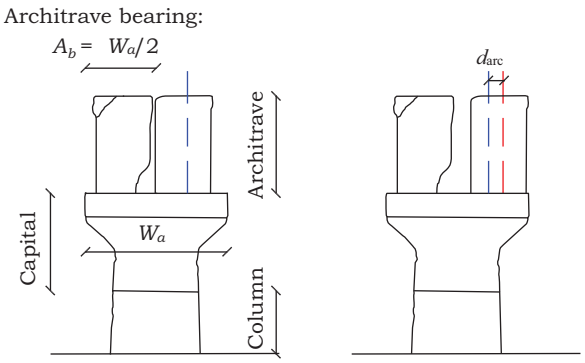

FIGURE 12 Definition of EDPs for architraves. Blue vertical lines indicate the initial position of the blocks while red lines their displaced (peak or residual) position.

TABLE 3 Performance criteria and associated limit states for columns and architraves; exceedance of either EDP threshold signifies violation of the respected LS.

Limit state (LS)	Monolithic column		Multi-drum column		Architrave		Performance level
	$\delta_{max,LS}$	$\delta_{res,LS}$	$\delta_{max,LS}$	$\delta_{res,LS}$	$\delta_{max,LS}$	$\delta_{res,LS}$	
LS1	0.25	0.15	0.25	0.15	0.25	0.15	Minor damage
LS2	0.50	0.30	0.50	0.30	0.50	0.35	Significant damage
LS3	1.00	1.00	1.00	1.00	1.00	1.00	Near collapse

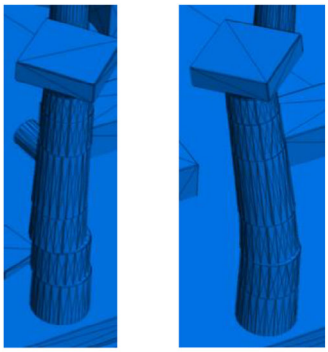

FIGURE 13 Typical dislocation of drums in a multi-drum column in case of exceeding (A) LS1 and (B) LS3.

4.3 | Limit states

Three performance levels were defined for each vulnerable structural element (monolithic column, multi-drum column, architrave). In the first level (LS1) that corresponds to minor damage, a seismic response with negligible rocking and sliding during the excitation is observed and no significant dislocation and damages of the blocks are expected at the end. The second level (LS2), corresponding to significant damage, pertains to significant normalized displacements, while the third level (LS3) is paired to a near collapse condition, corresponding to excessive displacement. The performance criteria and the associated limit states for monolithic and multi-drum columns, as well as architraves, are listed in Table 3. The values of the EDP thresholds were selected through a multiparametric investigation, including (a) engineering judgment, (b) assessment of the analysis results, (c) the work of Psycharis et al.,[17] and (d) previous published experimental results.[16,45,47] To provide a better understanding for the adopted EDP thresholds, the typical dislocation of drums in a multi-drum column is shown in Figure 13A for LS1 and in Figure 13B for LS3, while indicative conditions for the architraves with respect to the three LSs are depicted in Figure 14 in terms of residual transverse displacements.

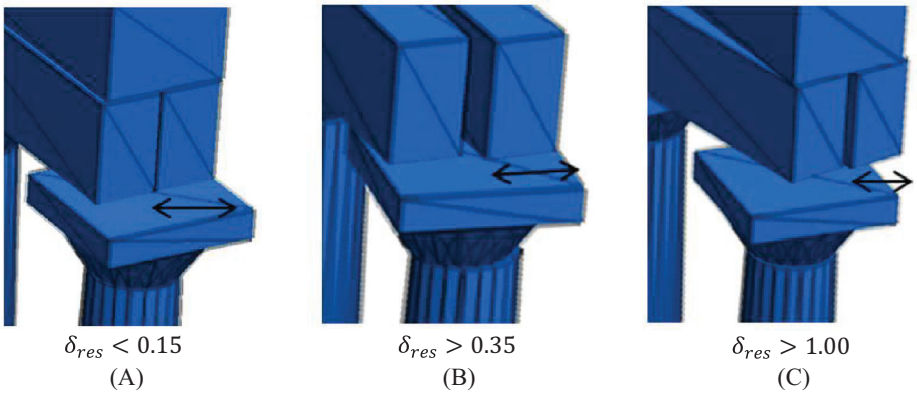

FIGURE 14 Typical dislocation in terms of residual normalized transverse displacement (δ_{res}) of architrave for the three limit states: (A) non-exceedance of LS1, (B) exceedance of LS2 signaling significant damage of the elements, (C) exceedance of LS3 denoting a near collapse situation.

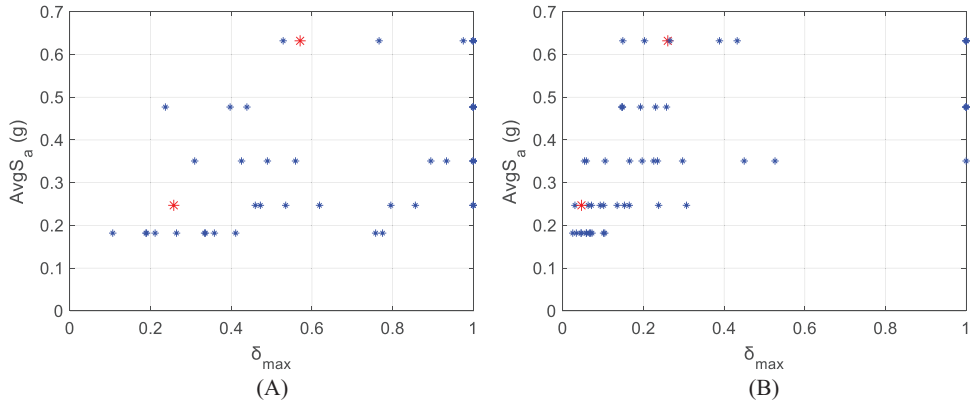

FIGURE 15 MSA results for δ_{max} as EDP (A) for the free-standing monolithic column K1 of the external colonnade and (B) the architrave EP1/2 of the Pronaos. Red stars indicate the analyses for which the response of the entire Temple is shown in Section 5.1.

5 | SESMIC RESPONSE ASSESESMENT

MSA[39] was employed for assessing the seismic response of the Temple by using the site-consistent ground motions selected for the hazard levels of Table 1. Indicative MSA results considering δ_{max} as EDP are illustrated in Figure 15A for the free-standing monolithic column K1 of the external colonnade and in Figure 15B for the architrave EP1/2 of the Pronaos (for the nomenclature of elements see Figure 10).

5.1 | Seismic response under single ground motions

To gain some intuition regarding the overall performance of the Temple, two characteristic examples of response under a single event are examined, namely, the Chi-Chi (1999) and the Northridge (1994) earthquakes properly scaled to the pre-defined Hazard levels of Table 1. In more detail, the state of the Temple at the end of the Chi-Chi (1999), CHY035-station ground motion scaled to Hazard Level 2 ($P_{50} = 10\%$ and return period equal to 475 years) is shown in Figure 16, where it is observed that all free-standing columns have been rotated, there are some misalignments of the architraves, but in general the colonnades have not suffered significant damage; any displacement and rotation of elements can be reversed in practice.

Then, for the excitation of Northridge (1994), Westmoreland station ground motion, scaled to Hazard Level 4 ($P_{50} = 1\%$ and return period equal to 4975years), the resulting condition of the Temple is shown in Figure 17. The main observation

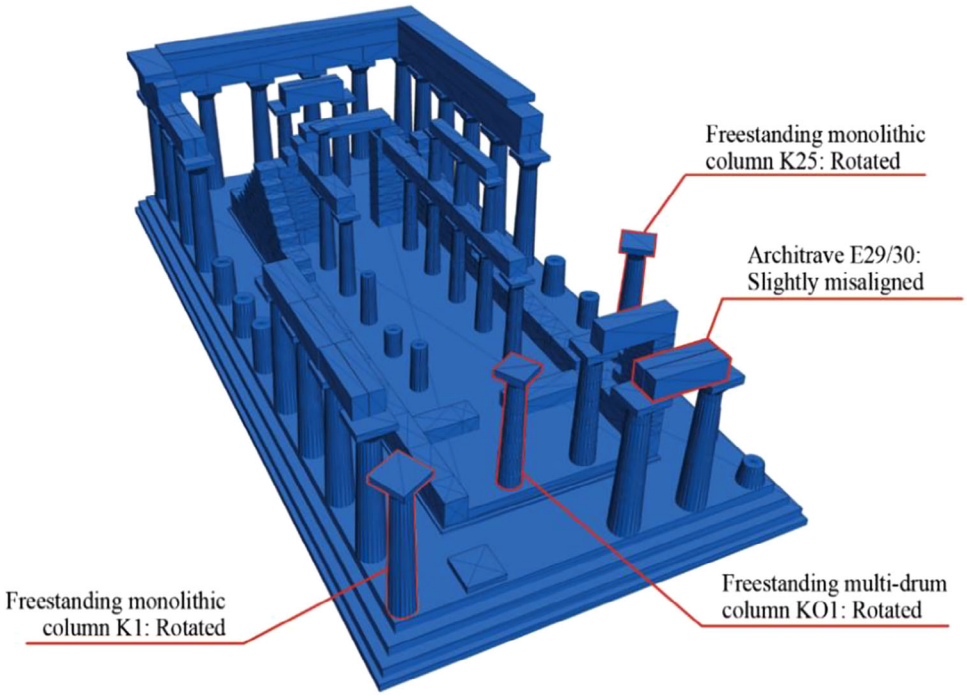

FIGURE 16 Condition of the Temple of Aphaia after it has been subjected to Chi-Chi (1999), CHY035 station ground motion scaled to Hazard Level 2 (P_{50} = 10% and return period equal to 475years).

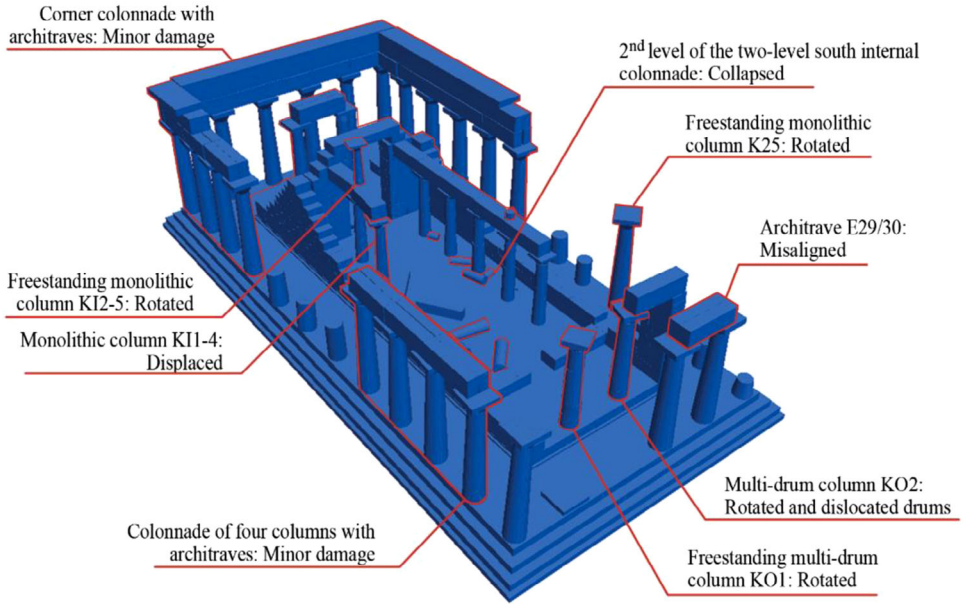

FIGURE 17 Deformed structural elements of the Temple of Aphaia subjected to the Northridge (1994), Westmoreland station ground motion scaled to the Hazard Level 4 (P_{50} = 1% and return period equal to 4975).

is that the colonnades are seismically resilient. Contrarily, the two-level colonnades of the Cella have suffered significant damage; in particular, the upper part of the south two-level colonnade (see Figure 10) has collapsed. The K25 monolithic free-standing column (see Figure 10 and Figure 3A) has significantly rotated, while the KO1 free-standing multi-drum column [see Figure 10 and Figure 3B] has suffered rotation, as well as, dislocation of the drums. It is worth noting that the two latter damages are significant but not catastrophic and can be essentially reversed. The KO2 multi-drum column connected to the Cella wall with architraves (see Figure 10 and Figure 3E) has undergone rotation and dislocation of

TABLE 4 Percentage of columns and architraves that exceed the predefined LS thresholds for two ground motions scaled to correspond to specific hazard levels.

		Columns			Architraves		
Seismic event	**Hazard level**	**LS1**	**LS2**	**LS3**	**LS1**	**LS2**	**LS3**
Chi-Chi 1999	10% in 50 years	3%	3%	0%	0%	0%	0%
Northridge 1994	1% in 50 years	27%	8%	11%	25%	3%	1%

TABLE 5 Range of the median $AvgS_a$, or μ_{50}, and the dispersion, β, of the lognormally fitted fragility curves for columns and architraves.

	Columns			Architraves		
Parameters	**LS1**	**LS2**	**LS3**	**LS1**	**LS2**	**LS3**
μ_{50} (g)	0.09–0.64	0.15–0.76	0.30–1.00	0.21–0.68	0.37–0.76	0.54–0.89
β	0.17–0.60	0.20–1.00	0.30–0.77	0.23–0.68	0.26–0.71	0.26–0.81
β_{tot}	0.26–0.65	0.27–1.05	0.32–0.80	0.30–0.71	0.33–0.74	0.33–0.83

drums. Moreover, slight transverse displacement of the architraves is in generally detected, as an opening can be observed between the two parts of the architraves in several locations (see example of Figure 12).

As a final remark, the percentage of columns and architraves that have exceeded the predefined LS thresholds for the two ground motions examined is listed in Table 4. Comparing the results obtained from the Hazard Level 2 ($P_{50} = 10\%$) event to the very rare Hazard Level 4 one ($P_{50} = 1\%$), the damage in the Temple differs significantly. Specifically, in the first case, practically all the structural elements of the Temple remained undamaged with only 3% of the columns exceeding the "Minor Damage" limit state and another 3% reaching Significant Damage. On the other hand, for the stronger ground motion, damages appear both in the columns and the architraves. Indicatively, it is obtained that ~25% of architraves exceeded the "Minor Damage" limit state, whereas ~11% of the columns suffered near collapse (exceedance of LS3).

5.2 | Seismic fragility assessment

Once the demand and capacity of the structural elements of the Temple have been evaluated, the next step is the fragility evaluation. Fragility curves are used to quantify the damage potential of a structure and are a key part of a seismic risk assessment study. More formal definitions of the seismic fragility can be found in[48,49]; it is essentially a function of the IM and provides the probability of exceeding a specific Limit State. Since both EDPs of δ_{max} and δ_{res} are employed to determine each LS, violation is defined at the exceedance of any of their respective thresholds, per Table 3:

$$F_{LS}(IM) = P\left[\delta_{max} > \delta_{max,LS} \text{ OR } \delta_{res} > \delta_{res,LS} \mid IM\right] \tag{4}$$

A single empirical fragility curve is thus calculated per structural element (column or architrave), in the form of an empirical cumulative distribution function (CDF). The resulting curves are presented in Figure 18 for some indicative elements of the Temple. Typically, an appropriate fitting is desired for the fragilities in order to facilitate the treatment of the problem and to extrapolate (within reason) the fragility beyond the IM-limit of analysis. Herein, a maximum likelihood estimation (MLE) lognormal fit[50] is applied to the empirical CDFs. The range of the median $AvgS_a$ values (μ_{50}) and the dispersion (standard deviation of the lognormal distribution, β) of the fitted fragilities per LS for the columns and the architraves of the Temple are presented in Table 5. The most vulnerable elements are the free-standing monolithic columns, K1 (shown in Figure 18A) and K25, indicating the beneficial contribution of the added weight by the architraves on the seismic stability of columns within colonnades (e.g., see[51]).

The resulting β only accounts for the record-to-record variability. Additional uncertainty should be introduced, for example, to account for the effects of the expert-opinion-based determination of Table 3 capacity thresholds or the use of a single "best-estimate" model for the structure under investigation. Lacking a careful quantification, which is beyond the scope of our study, literature values can be adopted. For conventional structures, recommended values can be found in pertinent guidelines (e.g., FEMA P58[52]). Contrarily, for the case of monumental structures no such guidance is available. Thus, for simplicity, an extra dispersion of 0.20 is assumed uniformly for all the elements and LS cases. This additional uncertainty is added to the β of the lognormally fitted fragilities per a first-order approximation, that is, assuming that it

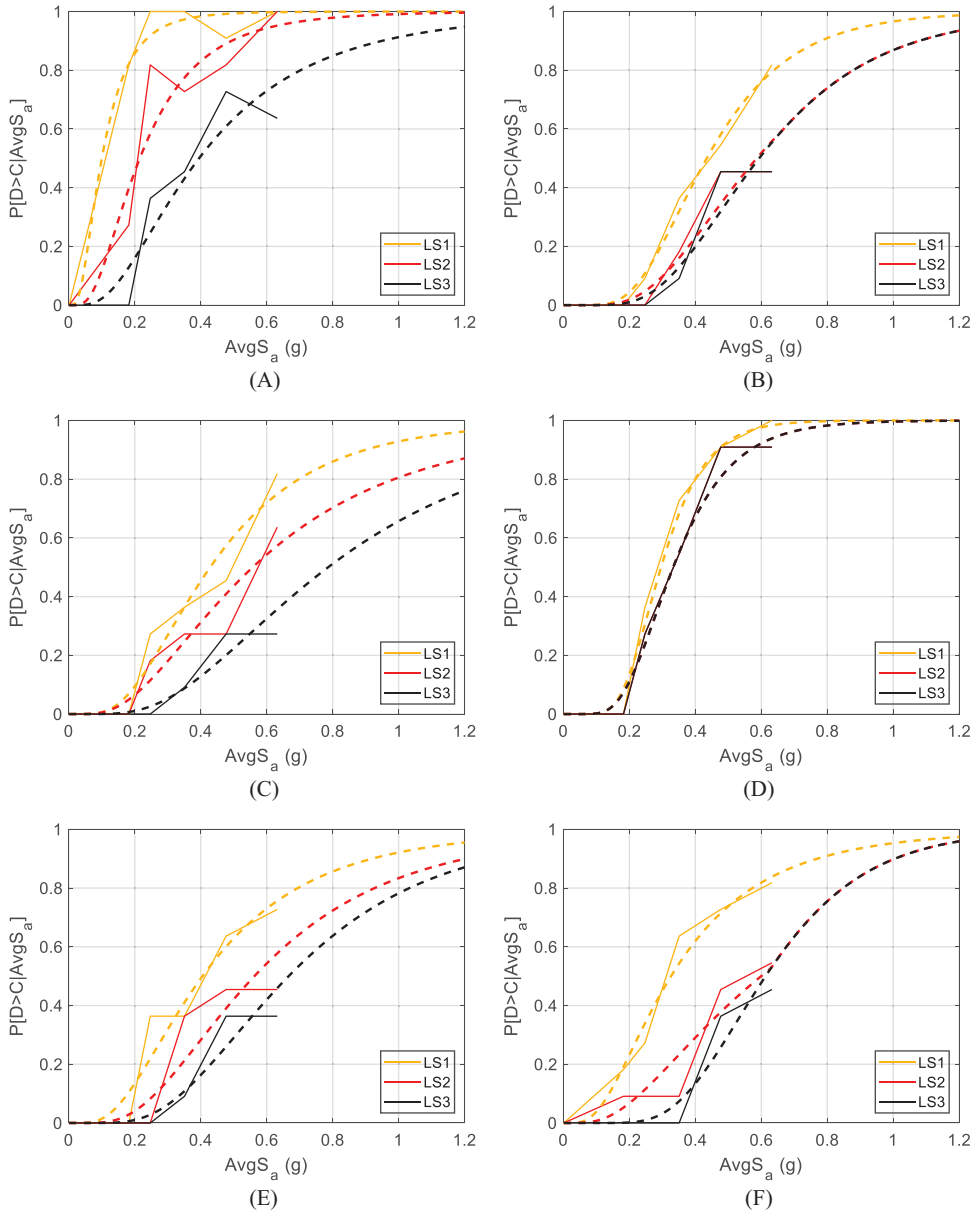

FIGURE 18 Indicative fragility curves of structural elements of the Temple of Aphaia: (A) free-standing monolithic column K1 of the external colonnade, (B) the architrave EP1/2 of the Pronaos, (C) column KI1-4 of the internal colonnade – first level, (D) column KI2-9 of the internal colonnade – second level, (E) architrave E2/3 of the external colonnade (columns in a row) f) architrave EI1/12 of the external colonnade (corner assemblage). Empirical fragility CDFs per LS are shown in solid lines, whereas the corresponding maximum likelihood lognormal fitted fragilities per LS are shown in dashed lines.

does not affect the mean and only inflates the dispersion:

$$\beta_{tot} = \sqrt{\beta^2 + 0.20^2} \tag{5}$$

As the β values are considerably higher than 0.20 for most elements and LS cases, this added dispersion only has a minor impact on the total dispersion (β_{tot}), as observed in Table 5. The lognormally fitted fragilities constructed using μ_{50}, β_{tot} for indicative elements of the Temple are depicted in Figure 18. It is observed that the adopted lognormal assumption is a fairly good fit in most cases. However, some differences can be identified in the lower tails of the fitted fragilities (low $AvgS_a$ levels) between the empirical and the fitted fragility CDFs. These are to be expected since the empirical CDFs are calculated by using limited sets of 11 records for a low number of hazard levels. For instance, no numerical analysis was

performed for $AvgS_a$ values between 0 and 0.18 g. Hence, a linear interpolation between 0 g and the first point of the empirical CDF at 0.18 g is employed, a choice that inevitably lowers accuracy. Accounting for more records per stripe or more hazard levels would certainly improve the empirical fragility CDFs at significant computational cost. Instead, we chose to accept this compromise and employ the lognormal fit to better capture the tails. The resulting differences, however small, will still tend to affect the estimated risk as they correspond to low IMs with high frequency of exceedance, λ_{AvgS_a} (see Figure 4).

As a final remark, the fitted fragilities were constructed by adopting a two-parameter lognormal model and thus some intersections between the lognormally fitted fragilities of different LSs can occur. To work around this issue, the worst LS result was adopted for any given level of $AvgS_a$, resulting to some lower fragilities coinciding with their higher LS ones for part of the IM range. For example, this is the case of the LS2 and LS3 fragilities for $AvgS_a > 0.6$ g in Figure 18F.

6 | SEISMIC RISK ASSESSMENT

The final step for the seismic performance assessment of the Temple is the assessment of risk. Herein, we focus on the long-term risk. Thus, the MAF of violating the i-th discrete limit state, λ_{LSi}, of Table 3 and the corresponding return period of exceedance $T_{r,i}$ were calculated by integrating the seismic fragility with the seismic hazard[27] by employing the lognormally fitted fragilities:

$$\lambda_{LSi} = \int_{IM} F_{LSi}(IM) \cdot |\mathrm{d}\lambda(IM)| \text{ with } i = 1, 2, 3 \tag{6}$$

$$T_{r,i} = \frac{1}{\lambda_{LSi}} \text{ with } i = 1, 2, 3 \tag{7}$$

A lower limit of $AvgS_a = 0.001$ g as set for the computation of the MAF in order to avoid recording damages for excessively low intensities. The long-term estimates in terms of return periods as obtained from Equations (6) and (7) are illustrated in Figure 19. Therein, the obtained return periods were grouped in order to offer a visual overview of the seismic risk. The return periods of exceeding LS1, which corresponds to minor damage, are shown in Figure 19A, while the return periods of exceeding LS3, which corresponds to the near collapse condition, are shown in Figure 19B. In both cases, the darker the color, the lower the return period for exceeding the corresponding LS and, consequently, the more prone to seismic damage the structural element is. In that sense, it is observed that the most vulnerable components are the free-standing columns (monolithic, multi-drum, and upper part of the internal colonnade) and the architraves of the internal colonnade, with return periods in the order of 20−500 years for LS1 and 300−2000 years for LS3. On the other hand, the external colonnade on the east part (i.e., the Pronaos, see Figure 3F), appearing in the back of Figure 19, will in general experience some low-level damage: return periods for LS1 of more than 2500 years, and for LS3 higher than 6000 years. In general, the return period for LS3 exceedance is of the order of hundreds or thousands of years for most elements.

Moving a step further in long-term risk, the MAF of exceeding percentages of total loss per group of elements (columns, architraves) was assessed. This was performed at the level of the MSA results, working on a record-by-record case to calculate the percentage of elements of the same type (columns, architraves) that exceed LS3. The total loss ratios of the columns and architraves are shown in Figures 20A and B, respectively, for the total number of the 5×11 records considered. In Figure 20, the corresponding 16/50/84% quantiles of the total loss ratio per IM level are also presented. On average, the architraves are less seismically vulnerable than the columns since the median total loss ratio is lower than that of the columns for all $AvgS_a$ levels. On the other hand, the total loss for the architraves shows higher dispersion than that of the columns.

Finally, the probability of exceeding the x loss level, denoted as $P[loss > x|IM]$, is calculated for given total loss ratio levels ranging from 0 to 1. Thus, the MAF of exceeding the x total loss ratio level is calculated as:

$$\lambda_{total\ loss}(x) = \int_{IM} P[loss > x|IM] \cdot |\mathrm{d}\lambda(IM)| \tag{8}$$

Again, for the integration with the hazard, the lower limit of $AvgS_a = 0.001$ g was employed for the integration per Equation (8). Figure 21 presents the MAF of the total loss ratio ($\lambda_{total\ loss}$) via Equation (8) for the columns and the architraves of the Temple. These estimates offer valuable information for prioritizing short- and long-term restoration actions. For example, for a return period $T_r = 475$ years, matching the design return period for ordinary structures per

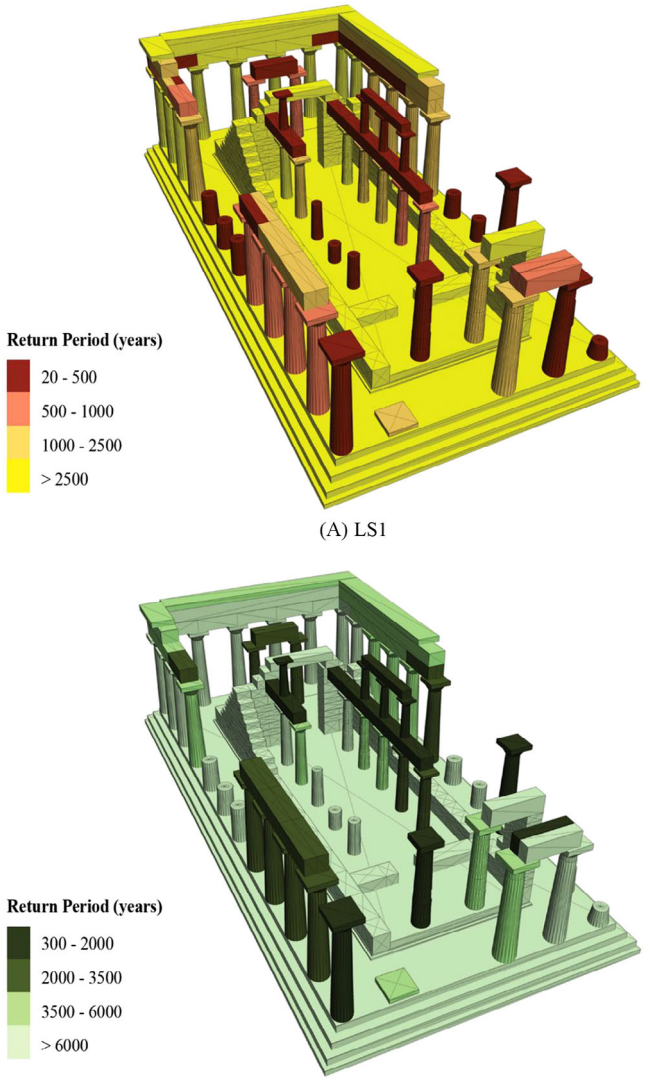

FIGURE 19 Range of the return periods (T_r) for exceeding: (A) LS1 ($T_{r,1}$) and (B) LS3 ($T_{r,3}$) for the elements of the Temple. Darker colors indicate lower return periods and consequently increased vulnerability.

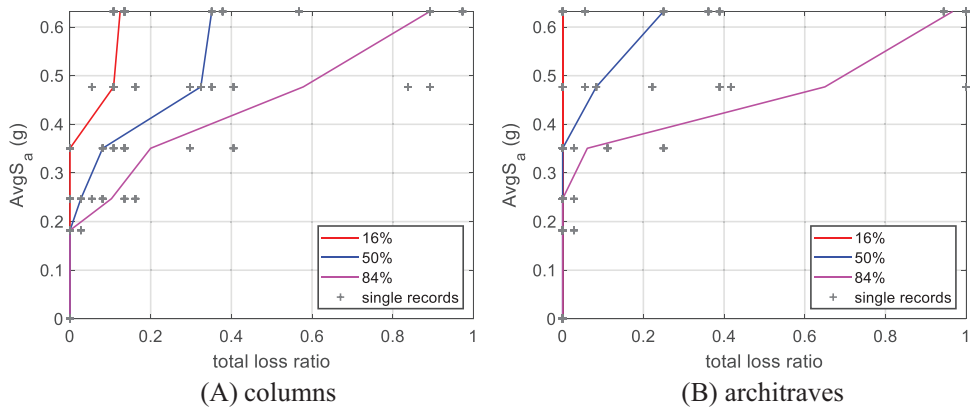

FIGURE 20 Total toss ratio per group of elements for the 5 × 11 ground motions employed and the corresponding 16/50/84% quantiles of total loss.

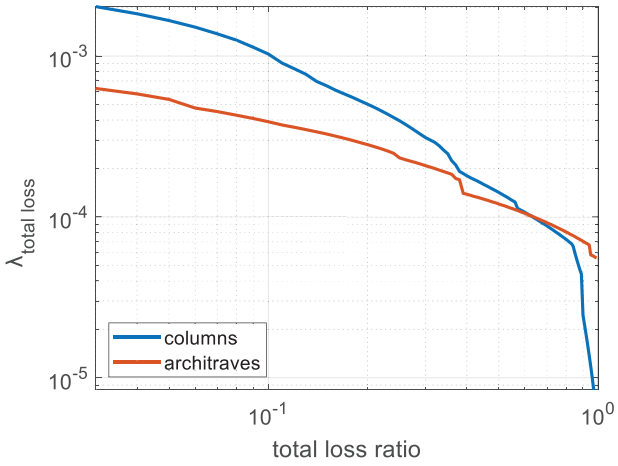

FIGURE 21 MAF of total loss for the columns and the architraves of the Temple.

EN 1998-1:2004,[40] the total loss ratio is 3% for columns and 0% for architraves. Instead, for a return period $T_r = 4975$ years, or the design return period for high-importance structures, the total loss ratio increases to 37% for columns and 30% for architraves.

7 | CONCLUSION

A seismic performance study of the ancient Temple of Aphaia in Aegina island, Greece has been presented. The remnants of the Temple today include free-standing columns, external colonnades, two-level internal colonnade, and walls. The numerical model of the Temple sub-assemblages was developed based on a point cloud obtained from UAV scanning. It was revealed that modeling ancient temples remains a challenge, even with advance Discrete Element Method software since the definition of the interface parameters requires judgement and some testing data that is not always available. Multi-stripe analysis was performed using a suite of appropriately selected hazard-consistent natural records. The fragility curves of the monument's structural elements were computed after proper engineering demand parameters and capacity thresholds were defined. The latter is a demanding task because the structural elements are not connected between them, due to their spinal configuration. A blend of criteria was employed for the definition of capacity thresholds, including among other previous studies, engineering judgment, test results, etc. Moreover, using a frugal assessment with few hazard levels and records is possible, but the construction of the fragilities may require some flexible fitting and careful post-processing to curtail the tails and remove any intersections. Finally, the long-term seismic risk of the individual structural elements was computed by convolving the seismic hazard with the fragility curves, revealing that the free-standing columns are the most seismically vulnerable elements, contrary to the colonnades. This process resulted in defining the return period of exceeding each Limit State for every structural element of the Temple. Such information is of significant importance for the Ephorate of Antiquities, which can prioritize the restoration actions and redistribute the financial sources for actions towards protecting the most vulnerable elements. Towards this direction, the mean annual frequency of exceeding percentages of total loss per group of elements, namely, columns and architraves, was assessed, revealing that architraves are more seismically resilience than columns.

ACKNOWLEDGMENTS

The authors would like to thank the ELXIS Group (https://www.elxisgroup.com/en/) for performing the 3D scanning of the Temple of Aphaia, which was funded by the Directorate of Restoration of Ancient Monuments, Ministry of Culture, Hellenic Republic, Athens, Greece. They also thank the Ephorate of Antiquities of Piraeus and Islands of the Ministry of Culture, Hellenic Republic, and Dr. Eleni-Eva Toumpakari from the Directorate of Restoration of Ancient Monuments, Ministry of Culture, Hellenic Republic for their help and support throughout the project. Finally, the authors acknowledge the help of Ms. Eirini Vourlakou in the preparation of the figures.

This research has been co-financed by the European Regional Development Fund of the European Union and Greek national funds through the Operational Program Competitiveness, Entrepreneurship and Innovation, under the call

RESEARCH—CREATE—INNOVATE (project code: T1EDK-00956), project: "ARCHYTAS: Archetypal telemetry and decision support system for the protection of monumental structures". Financial support has also been provided by the European Commission through the Horizon 2020 program "YADES—Improved Resilience and Sustainable Reconstruction of Cultural Heritage Areas to cope with Climate Change and Other Hazards based on Innovative Algorithms and Modelling Tools," Grant Agreement No. 872931.

DATA AVAILABILITY STATEMENT

The data that support the finding of this study are available from the corresponding author upon reasonable request.

ORCID

Maria-Eleni Dasiou https://orcid.org/0000-0003-3195-9575
Christos G. Lachanas https://orcid.org/0000-0001-9637-3482
Vasileios E. Melissianos https://orcid.org/0000-0002-1589-0697
Dimitrios Vamvatsikos https://orcid.org/0000-0002-4016-5040

REFERENCES

1. European Commission, Directorate-General for Education, Youth, Sport and Culture. European framework for action on cultural heritage, Publications Office, 2019. https://data.europa.eu/doi/10.2766/949707
2. Publisher Council of Europe. In: Bold J, Pickard R, eds. *An integrated approach to cultural heritage, The Council of Europe's Technical Co-operation and Consultancy Programme*. Council of Europe Publishing; 2018.
3. Sorrentino L, D'Ayala D, de Felice G, Griffith MC, Lagomarsino S, Magenes G. Review of out-of-plane seismic assessment techniques applied to existing masonry buildings. *Int J Archit Heritage*. 2017;11(1):1-20. doi:10.1080/15583058.2016.1237586
4. Clementi F, Gazzani V, Poiani M, Antonio Mezzapelle P, Lenci S. Seismic assessment of a monumental building through nonlinear analyses of a 3D solid model. *J Earthquake Eng*. 2018;22(sup1):35-61. doi:10.1080/13632469.2017.1297268
5. Cattari S, Camilletti D, D'Altri AM, Lagomarsino S. On the use of continuum finite element and equivalent frame models for the seismic assessment of masonry walls. *J Build Eng*. 2021;43:102519. doi:10.1016/j.jobe.2021.102519
6. Lagomarsino S, Cattari S, Ottonelli D. The heuristic vulnerability model: fragility curves for masonry buildings. *Bull Earthquake Eng*. 2021;19(8):3129-3163. doi:10.1007/s10518-021-01063-7
7. Lagomarsino S, Cattari S, Ottonelli D, Giovinazzi S. Earthquake damage assessment of masonry churches: proposal for rapid and detailed forms and derivation of empirical vulnerability curves. *Bull Earthquake Eng*. 2019;17(6):3327-3364. doi:10.1007/s10518-018-00542-8
8. Housner GW. The behavior of inverted pendulum structures during earthquakes. *Bull Seismol Soc Am*. 1963;53(2):403-417. doi:10.1785/BSSA0530020403
9. Yim C-S, Chopra AK, Penzien J. Rocking response of rigid blocks to earthquakes. *Earthq Eng Struct Dyn*. 1980;8(6):565-587. doi:10.1002/eqe.4290080606
10. Zhang J, Makris N. Rocking response of free-standing blocks under cycloidal pulses. *J Eng Mech*. 2001;127(5):473-483. doi:10.1061/(ASCE)0733-9399(2001)127:5(473)
11. Makris N, Konstantinidis D. The rocking spectrum and the limitations of practical design methodologies. *Earthquake Eng Struct Dyn*. 2003;32(2):265-289. doi:10.1002/eqe.223
12. Dimitrakopoulos EG, DeJong MJ. Revisiting the rocking block: closed-form solutions and similarity laws. *Proc R Soc A: Math Phys Eng Sci*. 2012;468(2144):2294-2318. doi:10.1098/rspa.2012.0026
13. Makris N, Kampas G. Size versus slenderness: two competing parameters in the seismic stability of free-standing rocking columns. *Bull Seismol Soc Am*. 2016;106(1):104-122. doi:10.1785/0120150138
14. Reggiani Manzo N, Lachanas CG, Vassiliou MF, Vamvatsikos D. Uniform risk spectra for rocking structures. *Earthquake Eng Struct Dyn*. 2022;51(11):2610-2626. doi:10.1002/eqe.3691
15. Lachanas CG, Vamvatsikos D. Rocking incremental dynamic analysis. *Earthq Eng Struct Dyn*. 2021;51(3):688-703. doi:10.1002/eqe.3586
16. Mouzakis HP, Psycharis IN, Papastamatiou DY, Carydis PG, Papantonopoulos C, Zambas C. Experimental investigation of the earthquake response of a model of a marble classical column. *Earthquake Eng Struct Dyn*. 2002;31(9):1681-1698. doi:10.1002/eqe.184
17. Psycharis IN, Fragiadakis M, Stefanou I. Seismic reliability assessment of classical columns subjected to near-fault ground motions. *Earthq Eng Struct Dyn*. 2013;42(14):2061-2079. doi:10.1002/eqe.2312
18. Kavvadias IE, Vasiliadis LK, Elenas A. Seismic response parametric study of ancient rocking columns. *Int J Archit Heritage*. 2017;11(6):791-804. doi:10.1080/15583058.2017.1298009
19. Sarhosis V, Baraldi D, Lemos JV, Milani G. Dynamic behaviour of ancient freestanding multi-drum and monolithic columns subjected to horizontal and vertical excitations. *Soil Dyn Earthquake Eng*. 2019;120:39-57. doi:10.1016/j.soildyn.2019.01.024
20. Ambraseys N, Psycharis IN. Earthquake stability of columns and statues. *J Earthquake Eng*. 2011;15(5):685-710. doi:10.1080/13632469.2010.541549
21. Ambraseys N, Psycharis IN. Assessment of the long-term seismicity of Athens from two classical columns. *Bull Earthquake Eng*. 2012;10(6):1635-1666. doi:10.1007/s10518-012-9388-1

22. Vayas I, Dasiou ME, Marinelli A. Säulen Griechischer Tempel Unter Erdbebenbeanspruchung. *Bautechnik*. 2007;84(6):388-396. doi:10.1002/bate.200710034
23. Makris N, Vassiliou MF. Planar rocking response and stability analysis of an array of free-standing columns capped with a freely supported rigid beam. *Earthq Eng Struct Dyn*. 2013;42(3):431-449. doi:10.1002/eqe.2222
24. Diamantopoulos S, Fragiadakis M. Modeling, fragility and risk assessment of ancient freestanding columns and colonnades. *Eng Struct*. 2023;275:115273. doi:10.1016/j.engstruct.2022.115273
25. Dasiou ME, Psycharis IN, Numerical investigation of the seismic response of Hephaestus Temple in Athens, Greece. *COMPDYN 2015 - 5th ECCOMAS Thematic Conference on Computational Methods in Structural Dynamics and Earthquake Engineering*, Chania, Greece; 2015. doi:10.7712/120115.3544.1233
26. Dasiou ME, Psycharis IN, Vayas I, Verification of numerical models used for the analysis of ancient temples. *International Conference on Protection of Historical Buildings, PROHITECH 09*, Rome, Italy; 2009.
27. Cornell CA, Krawinkler H. Progress and challenges in seismic performance assessment. *PEER Center News*. 2000;3(2):1-4. https://apps.peer.berkeley.edu/news/2000spring/performance.html
28. Webster TBL. The Temple of Aphaia at Aegina. *J Hell Stud*. 1931;51(2):179-183. doi:10.2307/626211
29. Gill DWJ. The temple of Aphaia on Aegina: further thoughts on the date of the reconstruction. *Annu Br Sch Athens*. 1993;88:173-181. https://www.jstor.org/stable/30064364
30. Furtwängler A, Fiechter ER, Thiersch H. *Aegina das Heiligtum der Aphaia*. Akademie der Wissenschaften in Kommission des G. Franz'schen Verlags (J. Roth); 1906.
31. Pagani M, Monelli D, Weatherill G, et al. Openquake engine: an open hazard (and risk) software for the global earthquake model. *Seismol Res Lett*. 2014;85(3):692-702. doi:10.1785/0220130087
32. Cornell CA. Engineering seismic risk analysis. *Bull Seismol Soc Am*. 1968;13(5):217-228. doi:10.1785/BSSA0580051583
33. Woessner J, Laurentiu D, Giardini D, et al. The 2013 European Seismic Hazard Model: key components and results. *Bull Earthquake Eng*. 2015;13(12):3553-3596. doi:10.1007/s10518-015-9795-1
34. Boore DM, Atkinson GM. Ground-Motion prediction equations for the average horizontal component of PGA, PGV, and 5%-damped PSA at spectral periods between 0.01 s and 10.0 s. *Earthquake Spectra*. 2008;24(1):99-138. doi:10.1193/1.2830434
35. Eads L, Miranda E, Lignos DG. Average spectral acceleration as an intensity measure for collapse risk assessment. *Earthq Eng Struct Dyn*. 2015;44(12):2057-2073. doi:10.1002/eqe.2575
36. Kazantzi AK, Vamvatsikos D. Intensity measure selection for vulnerability studies of building classes. *Earthq Eng Struct Dyn*. 2015;44(15):2677-2694. doi:10.1002/eqe.2603
37. Giouvanidis AI, Dimitrakopoulos EG. Rocking amplification and strong-motion duration. *Earthq Eng Struct Dyn*. 2018;47(10):2094-2116. doi:10.1002/eqe.3058
38. Lachanas CG, Vamvatsikos D, Dimitrakopoulos EG. Intensity measures as interfacing variables versus response proxies: the case of rigid rocking blocks. *Earthq Eng Struct Dyn*. 2023;52(6):1722-1739. doi:10.1002/eqe.3838
39. Jalayer F, Cornell CA. Alternative non-linear demand estimation methods for probability-based seismic assessments. *Earthq Eng Struct Dyn*. 2009;38(8):951-972. doi:10.1002/eqe.876
40. European Committee for Standardization. EN 1998-1:2004, Eurocode 8: Design of structures for earthquake resistance—Part 1: General rules, seismic actions and rules for buildings. Brussels, Belgium: European Committee for Standardization; 2004.
41. Kohrangi M, Bazzurro P, Vamvatsikos D, Spillatura A. Conditional spectrum-based ground motion record selection using average spectral acceleration. *Earthq Eng Struct Dyn*. 2017;46(10):1667-1685. doi:10.1002/eqe.2876
42. Kohrangi M, Bazzurro P, Vamvatsikos D, Spillatura A. Corrigendum to: conditional spectrum-based ground motion record selection using average spectral acceleration: conditional Spectrum-Based Record Selection (Earthquake Engineering & Structural Dynamics, (2017), 46, 10, (1667-1685), 1 0.1002/eqe.2876). *Earthquake Eng Struct Dyn*. 2018;47(1):265. doi:10.1002/eqe.2946
43. Jayaram N, Lin T, Baker JW. A computationally efficient ground-motion selection algorithm for matching a target response spectrum mean and variance. *Earthquake Spectra*. 2011;27(3):797-815. doi:10.1193/1.3608002
44. Ancheta TD, Darragh RB, Stewart JP, et al. PEER NGA-West2 Database. Berkeley, CA, USA: Pracific Earthquake Engineering Research Center, Technical Report PEER 2013/03; 2013. https://apps.peer.berkeley.edu/publications/peer_reports/reports_2013/webPEER-2013-03-Ancheta.pdf
45. Dasiou ME, Mouzakis HP, Psycharis IN, Papantonopoulos C, Vayas I. Experimental investigation of the seismic response of parts of ancient temples. *International Conference on Protection of Historical Buildings, PROHITECH 09*, Rome, Italy; 2009.
46. Itasca Consulting Group Inc. *3DEC: 3-Dimensional Distinct Element Code, Theory and Background*; 1998. https://www.itascacg.com/software/3DEC
47. Dasiou ME, Psycharis IN, Vayas I, Numerical investigation of the seismic response of Parthenon, Greece. *International Conference on Protection of Historical Buildings, PROHITECH 09*, Rome, Italy; 2009.
48. Bakalis K, Vamvatsikos D. Seismic fragility functions via nonlinear response history analysis. *J Struct Eng*. 2018;144(10):04018181. doi:10.1061/(ASCE)ST.1943-541X.0002141
49. Silva V, Akkar S, Baker J, et al. Current challenges and future trends in analytical fragility and vulnerability modeling. *Earthquake Spectra*. 2019;35(4):1927-1952. doi:10.1193/042418EQS101O
50. Baker JW. Efficient analytical fragility function fitting using dynamic structural analysis. *Earthquake Spectra*. 2015;31(1):579-599. doi:10.1193/021113EQS025M

51. Makris N, Vassiliou MF. Are some top-heavy structures more stable? *J Struct Eng*. 2014;140(5):06014001. doi:10.1061/(asce)st.1943-541x.0000933
52. Federal Emergency Management Agency. *FEMA P-58-1 Seismic Performance Assessment of Buildings*. vol. 1; 2018.

How to cite this article: Dasiou M-E, Lachanas CG, Melissianos VE, Vamvatsikos D. Seismic performance of the temple of Aphaia in Aegina island, Greece. *Earthquake Engng Struct Dyn*. 2023;1-20. https://doi.org/10.1002/eqe.4032